JACS
JOURNAL OF THE AMERICAN CHEMICAL SOCIETY
pubs.acs.org/JACS
Article

Turn-on Fluorescent Biosensors for Imaging Hypoxia-like Conditions in Living Cells

Santiago Guisán-Ceinos, Alexandra R. Rivero, Fernando Romeo-Gella, Silvia Simón-Fuente, Silvia Gómez-Pastor, Natalia Calvo, Alejandro H. Orrego, José Manuel Guisán,* Inés Corral,* Francisco Sanz-Rodriguez,* and Maria Ribagorda*

Cite This: J. Am. Chem. Soc. 2022, 144, 8185–8193
Read Online

ABSTRACT: We present the synthesis, photophysical properties, and biological application of nontoxic 3-azo-conjugated BODIPY dyes as masked fluorescent biosensors of hypoxia-like conditions. The synthetic methodology is based on an operationally simple N═N bond-forming protocol, followed by a Suzuki coupling, that allows for a direct access to simple and underexplored 3-azo-substituted BODIPY. These dyes can turn on their emission properties under both chemical and biological reductive conditions, including bacterial and human azoreductases, which trigger the azo bond cleavage, leading to fluorescent 3-amino-BODIPY. We have also developed a practical enzymatic protocol, using an immobilized bacterial azoreductase that allows for the evaluation of these azo-based probes and can be used as a model for the less accessible and expensive human reductase NQO1. Quantum mechanical calculations uncover the restructuration of the topography of the S_1 potential energy surface following the reduction of the azo moiety and rationalize the fluorescent quenching event through the mapping of an unprecedented pathway. Fluorescent microscopy experiments show that these azos can be used to visualize hypoxia-like conditions within living cells.

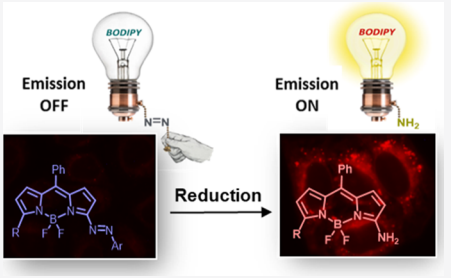

INTRODUCTION

Azobenzenes have emerged as outstanding fluorescent quenchers used for biosensing and bioimaging studies.[1,2] Following its coupling, the azo moiety is able to extinguish the emission of several fluorophores by a nonradiative process operating under the Förster resonance energy transfer (FRET) mechanism or by a non-FRET process generally associated with the ultrafast trans/cis N═N bond isomerization.[3] The fluorescence of these azo-based quenching dyes can be activated by chemical or biological reductants (*i.e.*, azoreductases)[4] that trigger the cleavage of the N═N azo moiety, releasing the fluorescent probe and allowing for the easy tracking of biological events by fluorescence microscopy.[5] The reversibility of the first half-reduction of the azo N═N double bond is highly dependent on the oxygen in the medium. Thus, in reducing media and in the absence of oxygen, such as hypoxia-like conditions, the azo compounds can suffer an irreversible reductive breakdown of the N═N bond, releasing the fluorophore. Nagano *et al.*[6] originally reported a nonemissive fluorophore probe based on the azo Black Hole Quencher (BHQ-3) for the detection of acute ischemic and related hypoxia diseases.[7,8] From this seminal work, a series of azocompounds, conjugated with other fluorophores, have been reported to inhibit different emission wavelengths and to detect different levels of hypoxia and acute ischemia.[9−11] Although the use of azocompounds as fluorescent quenchers is well known, to the best of our knowledge, there has been no attempt to conjugate an azo moiety to a BODIPY by the C-3 position. This simple azo quencher would be useful for the development of novel sensors for hypoxia-like conditions because reductive cleavage of the azo bond would re-establish the outstanding emission properties of the BODIPY[12] moiety.

Herein, we report the synthesis of 3-arylazo-BODIPY, prepared under very mild conditions from 3,5-dichloro-BODIPY and commercially available *p*-benzoquinone bisketal (Figure 1). The initial nonemissive azo-conjugated BODIPY accommodates a chloro substituent, amenable for chemical modification, providing a handle for further functionalization and modulation of the final photophysical properties. The fluorescence is turned on under chemical or enzymatic (*i.e.*, azoreductase) reductive conditions and also visualized in HeLa cells under hypoxia-like conditions by fluorescence imaging techniques. Quantum mechanical calculations provide a novel insight into the molecular origin of the quenching event and rationalize the photophysical properties of both azo dyes and the released amino fluorophores.

Received: January 30, 2022
Published: April 29, 2022

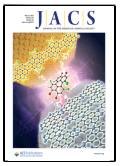

https://doi.org/10.1021/jacs.2c01197
J. Am. Chem. Soc. 2022, 144, 8185−8193

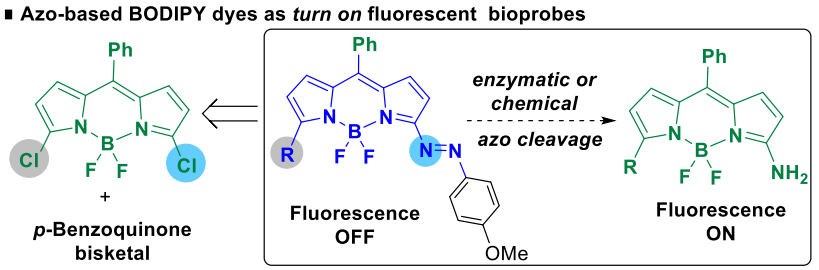

Figure 1. Design of nonfluorescent 3-azo-BODIPY and fluorescent 3-amino-BODIPY dyes.

Scheme 1. Synthesis of Azo-BODIPY Dye 3 from 1

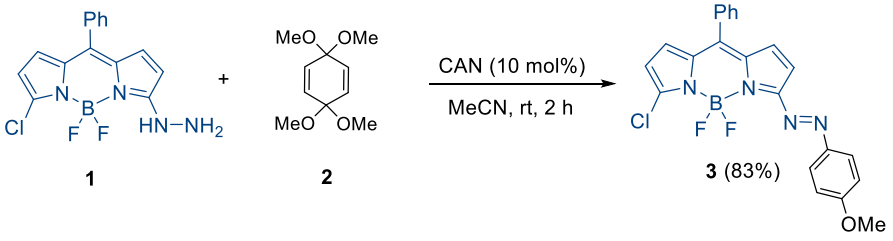

Scheme 2. One-Pot Synthesis of 3 and Preparation of 5

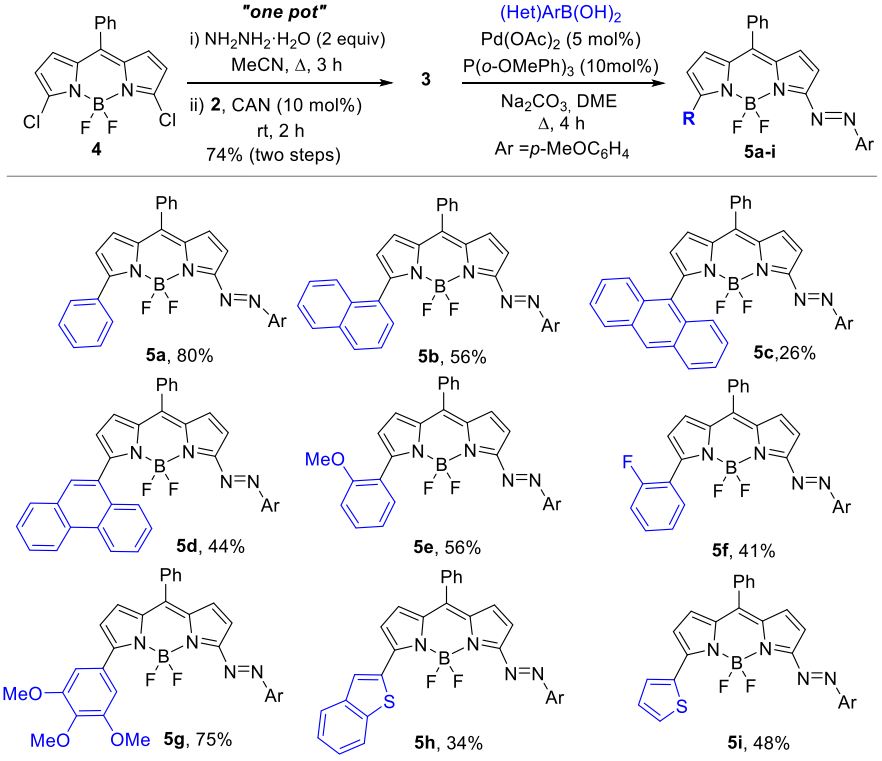

RESULTS AND DISCUSSION

Generally, azo-based nonemissive fluorophores are prepared by azo-coupling reactions, between *in situ* generated aryldiazonium salts and electron-rich aromatic compounds, or by a Mills reaction, from nitroso derivatives and aromatic amines. In a previous work, we reported the synthesis of azo derivatives based on reactions of arylhydrazines with quinone bisketals.[13] In contrast to conventional methods known for making azo derivatives, this strategy avoids using strong acids or base reagents and only requires catalytic amounts of cerium ammonium nitrate (CAN).[14,15] To examine whether our methodology could be extended to the preparation of more complex heterocyclic (BODIPY) azo derivatives, we studied the reaction between hydrazine-BODIPY **1** and the commercially available bis-dimethyl acetal of *p*-benzoquinone **2**. To our delight, the reaction using CAN as the catalyst at rt gave the desired azo derivative **3** as a nonfluorescence dark blue solid in 83% isolated yield (Scheme 1).

Gratifyingly, the method was improved following an operationally simple two-step strategy, starting from 3,5-dichloro-BODIPY[16] **4** by the sequential addition of hydrazine followed by the addition of **2** and CAN. This procedure avoided the isolation of hydrazine-**1** and decreased the amount of hydrazine required for its preparation[17] (Scheme 2). Notably, the remaining 5-

https://doi.org/10.1021/jacs.2c01197
J. Am. Chem. Soc. 2022, 144, 8185−8193

Scheme 3. Synthesis of 3-Amino-BODIPY Dyes 6

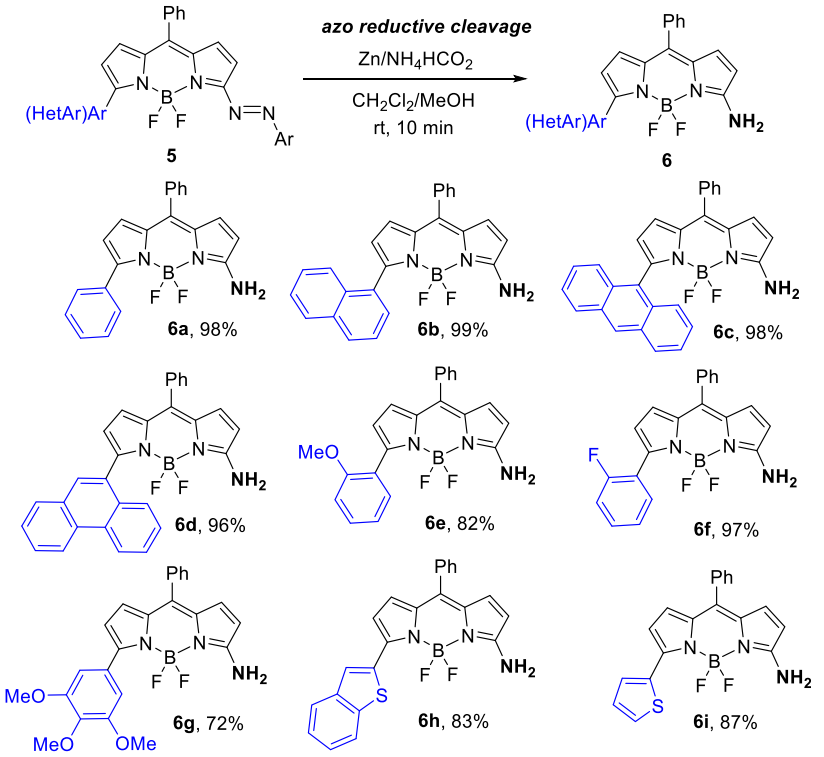

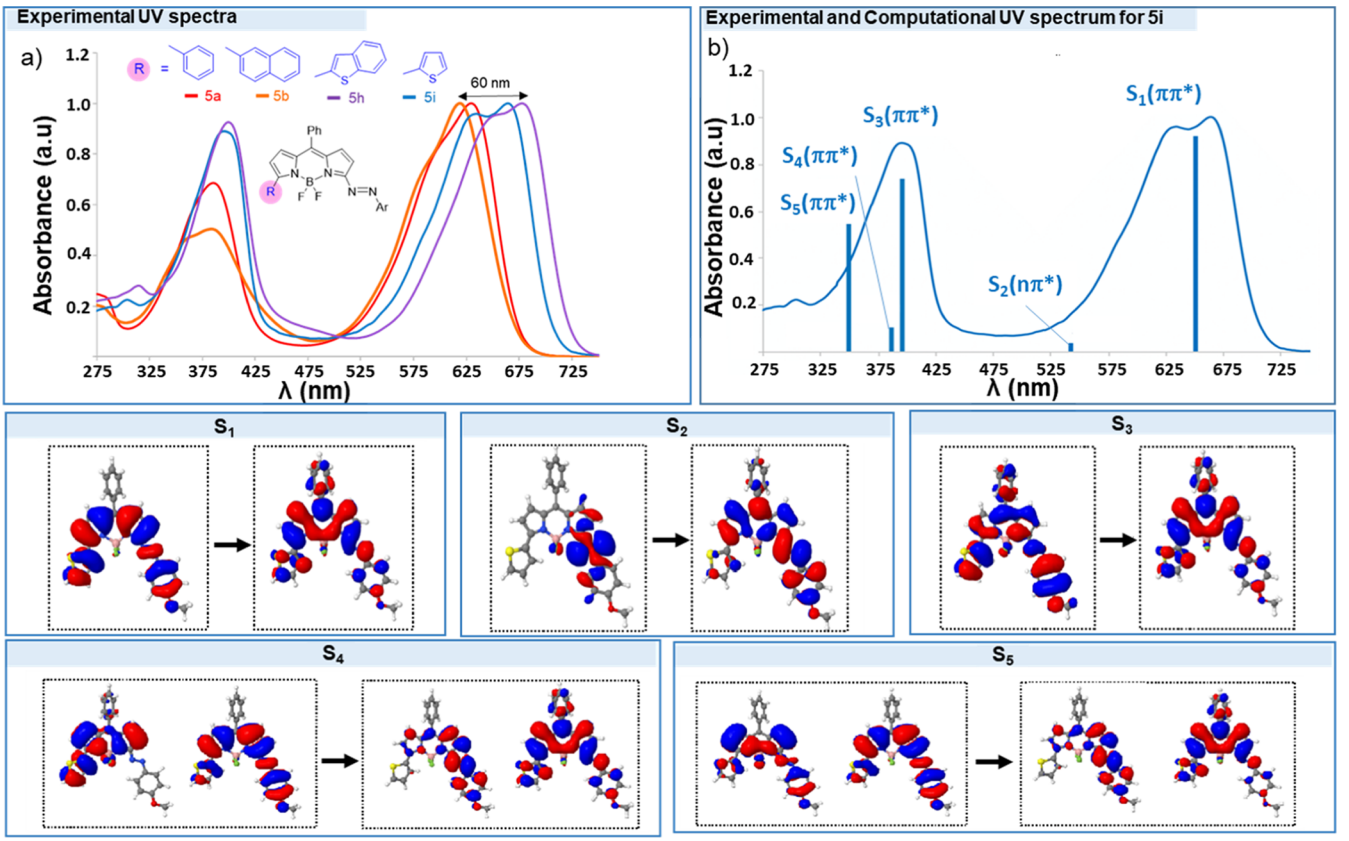

Figure 2. (Top) (a) Experimental absorption spectra of representative **5a,b** and **5h,i** derivatives in DCM. (b) RI-ADC(2)/def2-SVP vertical excitation energies superimposed to the experimental *trans*-azo **5i** absorption spectra (red-shift applied 0.38 eV). (Bottom) Natural transition orbitals for the lowest-lying excited electronic states S_1−S_5 contributing to the main absorption bands of **5i**.

https://doi.org/10.1021/jacs.2c01197
J. Am. Chem. Soc. 2022, 144, 8185−8193

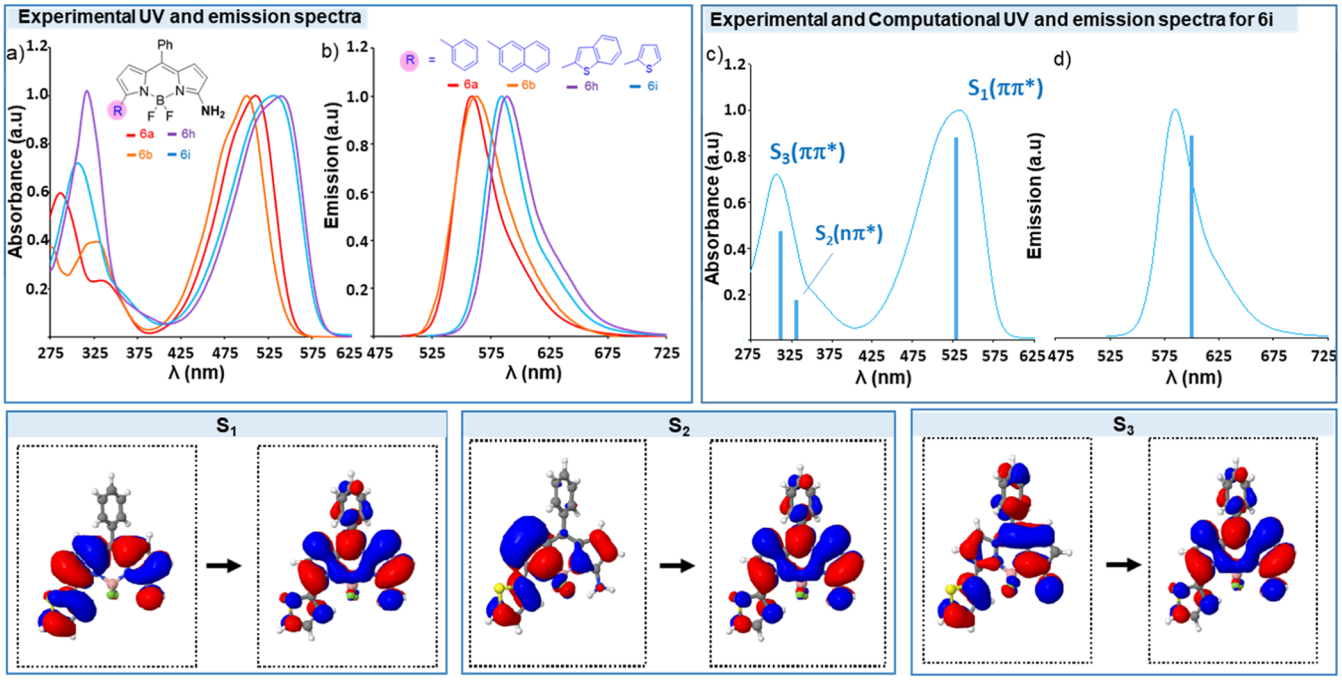

Figure 3. (Top left) Experimental (a) absorption and (b) emission spectra of representative derivatives in DCM exciting (λ_{ex}) at 511 nm (**6a**), 500 nm (**6b**), 531 nm (**6h**), and 525 nm (**6i**). (Top Right) RI-ADC(2)/def2-SVP vertical energies superimposed to the experimental (c) absorption and (d) emission spectra of **6i** (red-shift applied 0.14 eV). (Bottom) Natural transition orbitals for the lowest-lying excited electronic states S_1−S_3 involved in the main absorption and emission bands.

chloro substituent allowed to increase the chemical diversity and electronic properties accessible by a Suzuki cross-coupling reaction (Scheme 2).[18]

The feasibility of the cross-coupling reaction was initially studied using 5-chloro-3-arylazo-BODIPY **3** and phenyl boronic acid. After screening different palladium salts and phosphine ligands,[19] the best yield was obtained using $Pd(OAc)_2$ as the catalyst, $P(2\text{-MeOPh})_3$ as the ligand, and Na_2CO_3 as the base in DME at reflux for 4 h,[20] isolating **5a** in 80% yield.

Following these conditions, several aryl and heteroaryl groups were engaged. Condensed aromatic boronic acids, such as naphthyl, anthracenyl, and phenantryl, afforded the desired compounds. Electron-rich and electron-poor aryl boronic acids and heterocyclic 2-benzothienyl and 2-thienyl derivatives were also well tolerated and gave the desired products in moderate to good yields. All these new 3-arylazo-BODIPY derivatives were dark blue solids, lacking fluorescence emission.

To examine the potential of azo-BODIPY **5** as a fluorescent turn-on probe under reductive conditions, we initially undertook the reductive azo bond cleavage by treating **5a**−**i** with zinc and ammonium formate (Scheme 3). In all cases, the corresponding 3-amino-derivatives **6a**−**i** were successfully formed in excellent yields. A remarkable color change was observed almost immediately, from an initially dark blue solution to a fluorescent green to orange-yellow solution.

Next, we studied the photophysical properties of the 3-arylazo-BODIPY **5** and 3-amino-BODIPY **6** using CH_2Cl_2 as the solvent (see Tables S2 and S3). The UV spectra of representative examples (**5a,b** and **5h,i**) are shown in Figure 2 (top a). The absorption spectra of **5** correspond to a red-shifted version of the combined chromophores (BODIPY and azobenzene). In general, two absorptions bands appear at 619−679 nm and in the UV region (~370−400 nm). The maximum absorption band can be shifted up to 60 nm depending on the C-5 substituent. The thienyl derivatives **5h** (λ_{abs} 679 nm) and **5i** (λ_{abs} 665 nm) displayed the most red-shifted bands. As expected, azo-BODIPY **5** showed negligible fluorescence emission (see Figure S3 for a representative emission spectra of **5i**).

A detailed analysis of the nature of the two characteristic absorption bands on the most stable *trans*-azo isomer of **5i**, based on the scrutiny of the natural transition orbitals, reveals that the electronic transitions in these systems cannot be longer ascribed either to the BODIPY or the azobenzene moiety separately, but instead both fragments are involved in the electronic excitation; see Figure 2 (top b and bottom). In particular, the first absorption at 630−700 nm, which is assigned to the S_1, corresponds to a $\pi\pi^*$ transition localized along the BODIPY and azo aryl moieties. We ascribe the second absorption at 370−380 mainly to the $\pi\pi^*$ S_3 and S_5 states, also delocalized on the BODIPY and the azobenzene moieties, although the predominant contribution in the case of S_3 and S_5 is from the azobenzene fragment and the BODIPY, respectively (see Figures 2b and S6). Our calculations predict the characteristic $n\pi^*$ transition of the azobenzene as the dark state peaking at *ca.* 467 nm (S_2).

On the contrary, the 3-amino-BODIPY derivatives **6** exhibit an intense emission fluorescence in the green-red range λ_{em} 552−589 nm (see Figure 3b for representative examples, Table S3 and Figure 3d for theoretical calculations of **6i**).

The UV−vis spectra of **6** show a maximum absorption at 493−531 nm (Figure 3a), calculated for **6i** at λ 500 nm and assigned to $S_1(\pi\pi^*)$ (Figure 3c). This band is characteristic of the BODIPY and is mainly localized over the pyrrole and thienyl rings (Figure 3 bottom S_1). The substitution pattern at C-5 alters the position of both the absorption (up to 60 nm shift) and emission (up to 37 nm shift) maxima. Compounds **6h** (λ_{em} 589) and **6i** (λ_{em} 585) have the most red-shifted emission. For the

https://doi.org/10.1021/jacs.2c01197
J. Am. Chem. Soc. 2022, 144, 8185−8193

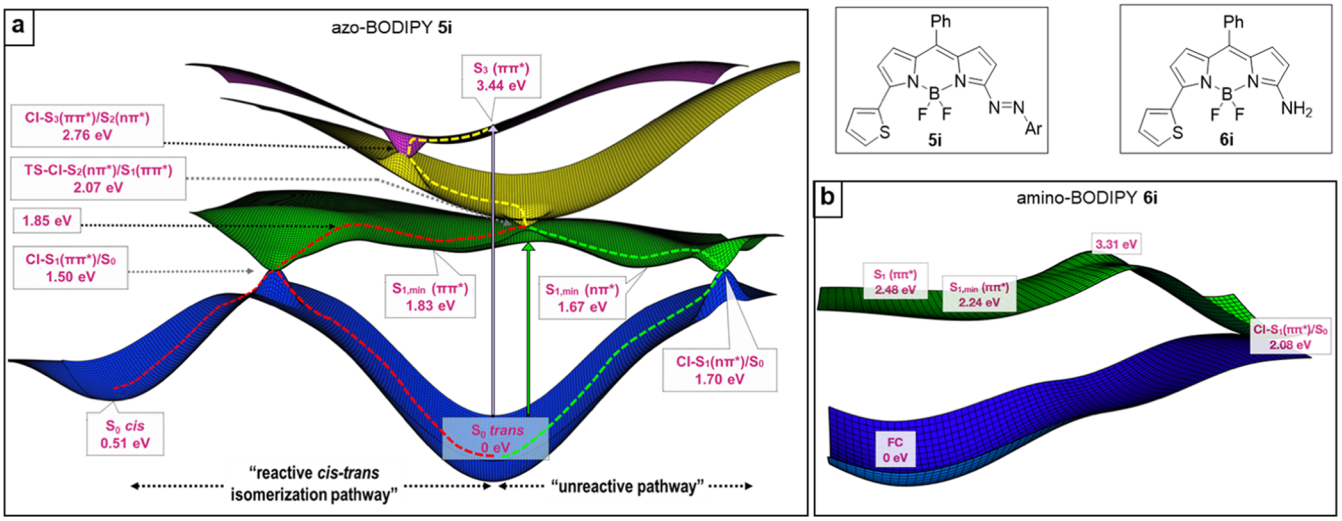

Figure 4. Potential energy landscape of (a) azo-BODIPY **5i** and (b) amino-BODIPY **6i** obtained at the RI-ADC(2)/def2-SVP level of theory.

biological studies, the UV−vis and emission spectra of **6i** were also measured in a PBS/DMSO solution, showing values of λ_{abs} = 500 nm and λ_{em} 585 nm. The fluorescence quantum yields (Φ) of **6** varied from 0.24 to 0.95 (Table S3). The highest values were obtained for the thienyl derivatives **6h** (Φ 0.91) and **6i** (Φ 0.95 in DCM and 0.4 in DMSO/PBS). The Stokes shifts are significantly large (from 50 to 85 nm, Table S3) for a BODIPY derivative, which is very interesting to allow for high-sensitivity bioimaging.[21] All these results confirmed that the azo group situated at C-3 position of the BODIPY acts as a strong fluorescence quencher and that the 3-amino-BODIPY **6**, obtained upon the reductive azo cleavage, successfully recovers the BODIPY emission.

The photophysical properties of the 3-azo-BODIPY and the 3-amino-BODIPY derivatives can be readily explained from the topography of the excited potential energy surfaces along the coordinates relevant to the deactivation of these systems (Figure 4). Interestingly, the coupling of the azo moiety to the BODIPY dramatically modifies the landscape of the excited state potential energy surface of the fluorophore. In fact, the deep S_1 minimum characteristic of the parent BODIPY compound and its meso substituted derivatives[22a−c] (Figure 4b), responsible for the remarkable fluorescence of these species, is replaced in the azo-BODIPY system (Figure 4a), by two very shallow minima, $S_{1,min}(\pi\pi^*)$ and $S_{1,min}(n\pi^*)$, in the same potential (accessible after irradiation at 630−700 nm). The first minimum, located in the vicinity of the Franck−Condon region (FC), and thus very similar to the trans ground state isomer, presents $\pi\pi^*$ character, while the second of $n\pi^*$ nature would present overstretched CNN angles (see stationary geometries in Figure S9). A quite small barrier separates both minima, ensuing the exchange of population between them. For its part, a rather planar potential connects these minima with two internal conversion funnels, CI-$S_1(\pi\pi^*)/S_0$ and CI-$S_1(n\pi^*)/S_0$, as shown in Figure 4, (CI = conical intersection). CI-$S_1(\pi\pi^*)/S_0$ defining the "reactive pathway" would bifurcate the population between the cis-S_0 and trans-S_0 minima (see Figure 4a, red line path), while CI-$S_1(n\pi^*)/S_0$ would exclusively return the population to the original S_0 trans minimum by the pathway name "unreactive" (see Figure 4a, green line path). The accessibility of the CI-$S_1(\pi\pi^*)/S_0$ and CI-$S_1(n\pi^*)/S_0$ internal conversion funnels from the S_1 minima is consistent with the absence of fluorescence experimentally observed for these systems.

Our minimum energy path calculations also predict a downhill potential energy profile from S_3 (state predominantly accessed after 370−380 nm irradiation) to S_1. Specifically, decay from S_3 would direct the population first toward the CI-$S_3(\pi\pi^*)/S_2(n\pi^*)$ crossing and then to the CI-$S_2(n\pi^*)/S_1(\pi\pi^*)$ crossing (Figure 4a, yellow line path), the latter located near the S_1 transition state connecting the $\pi\pi^*$and $n\pi^*$ minima, TS ($\pi\pi^*$−$n\pi^*$). This crossing is expected to distribute population between the two $S_{1,min}(\pi\pi^*)$ and $S_{1,min}(n\pi^*)$ minima. The exclusive experimental identification of the *trans*-azo-BODIPY isomer, following irradiation of the azo-BODIPY **5i** either with red, green, or UV photons, discards the potential deactivation of the system through the expected ultrafast trans/cis isomerization CI-$S_1(\pi\pi^*)/S_0$ funnel (Figure 4a, red line path) and points to S_3FC → CI-S_3/S_2 → CI-S_2/S_1 → [$S_{1,min}(\pi\pi^*)$] → $S_{1,min}(n\pi^*)$ → CI-$S_1(n\pi^*)/S_0$ → trans-S_0 as the most probable decay mechanism for this system (Figure 4a, green line path).

However, in view of the similar energetics accessibility of both deactivation paths, we infer that the preference for the unreactive mechanism can be only attributed to dynamical effects, which can only be accounted for when undertaking molecular dynamics simulations. The preference, although no exclusiveness, for the nonreactive pathway has been actually observed in previous works on the simpler azobenzene system, which presents a very similar flat S_1 potential energy surface along the $n\pi^*$ and $\pi\pi^*$ coordinates.[22d] The restoration of the characteristic fluorescent properties of BODIPY upon the reduction of the azo group is also imprinted in the potential energy surfaces of the reduced species. As can be seen in Figure 4b, the population of the 3-amino-BODIPY **6i** excited to S_1 would be directed toward a planar $S_{1,min}$, vertically located at 574 nm (observed λ_{em} 552−589 nm). Moreover, in this case, the nonradiative decay of the population is hindered by an activation barrier that intercalates the minimum from the CI-$S_1(\pi\pi^*)/S_0$ conical intersection. Interestingly, while CI-S_1/S_0 for the amino-BODIPY shares some structural similarity to the most stable CI computed for the parent BODIPY,[22b,c] that is, butterfly folding along the C8−B axis and the tilting of the group/H located at the meso position, C3-functionalization of the BODIPY core alters the energetics of the decay paths of the chromophore. In

https://doi.org/10.1021/jacs.2c01197
J. Am. Chem. Soc. 2022, 144, 8185−8193

particular, the incorporation of an amino group at C3 shifts CI-S_1/S_0 below the energy of the minimum, while the inaccessibility of the S_1/S_0 funnel and thus the fluorescent properties are preserved due to the existence of a barrier between the minimum and CI.

Next, we studied the potential use of these azo-BODIPY as turn-on fluorescent biosensors of reductive media. To this aim, the enzymatic reduction of azo-BODIPY **5** was studied using two different azoreductases capable of cleaving azo bonds, using nicotinamide adenine dinucleotide (NADH) or flavin-adenine-dinucleotide (FAD) as cofactors. Specifically, we tested the bacterial *Bacillus cereus* azoreductase (*azoRBC*) and a human NADH-quinone oxido-reductase (NQO1). The enzymatic reduction was initially tested with azo-BODIPY **5i**, and the azoreductase activity was measured as a function of the decrease in the intensity of the 615 nm absorption band (absorption maxima using H_2O/EtOH 1:1). As a reference, the enzymes activities were evaluated with commercially available Methyl Red azocompound (λ_{abs} 430 nm), that is known to be cleaved by these enzymes. Bacterial *azoRBC* is a homodimeric enzyme of low molecular weight (21.5 kDa for each subunit), with optimum working conditions at pH 6−7 at 40 °C. Due to the low solubility of **5i** in aqueous enzymatic medium, the photophysical properties were measured in a 1:1 H_2O/EtOH mixture, which allowed for increasing the substrate concentration 10 times (**5i** from ≈2.5 to 25 μM) and the reduced product concentration more than 10 times. However, in this solvent mixture, the bacterial *azoRBC* formed aggregates, inactivating and preventing the total reduction of the substrates (see Table S4). To avoid such inactivation, the enzyme was immobilized on a solid support (agarose gel) coated with polyethyleneimine (PEI). *azoRBC* was immobilized (*i-azoRBC*) by an adsorption method promoted by the ionic exchange between several carboxyl groups of each enzyme molecule and several ionized amino groups of a PEI-coated agarose support (Figure S13). Thus, the highly hydrophilic environment surrounding each enzyme molecule can also protect it from other negative effects promoted by the presence of EtOH that is necessary to solubilize substrates and products. The immobilization was complete in less than 1 h, retaining 100% of the activity, and *i-azoRBC* contains 0.33 mg of enzyme per gram of the catalyst (see Figure S14). The stability study comparing the free and the immobilized enzyme incubated in H_2O/EtOH (1:1) showed that *i-azoRBC* was much more stable and retained more than 90% of its activity after 50 h, whereas the free enzyme was rapidly inactivated, and so, it would not be feasible to do long reduction tests (see Figure S15).

The reduction process was carried out in the presence of the reducing cofactor, NADH, and monitored by the decrease of absorbance at 615 nm for **5i**. Without NADH, the absorbance remains unaltered, and after its addition, it decreases to 0.001 in 4 min (see Figures 5 and S16). In the absence of the enzyme, the addition of NADH to **5i** does not modify the absorbance at 615 nm. These results indicate that the release of the fluorophore must occur by an enzyme reductive cleavage pathway.

The activity of the immobilized enzyme against a selection of azo-BODIPY derivatives and the activity percentage (considering 100% the activity with Methyl Red) are depicted in Table 1. The enzyme *i-azoRBC* showed very good results for **5c** (125%, Table 1, entry 4) and **5f** (110%, entry 6), good for other derivatives such as 5-chloro-arylazo BODIPY **3** (80%, entry 3) and moderate for the *ortho*-methoxy derivative **5e** (30%, entry 5).

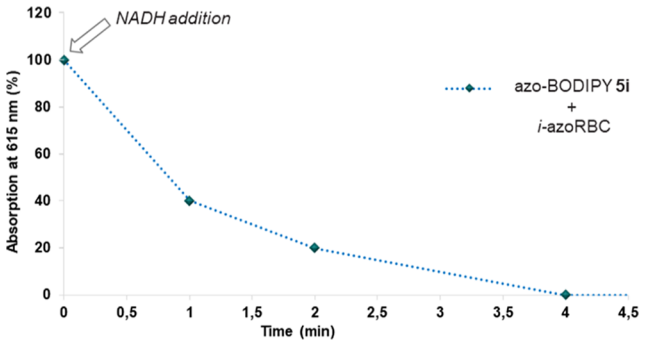

Figure 5. Time-course of the enzymatic reduction of azo-BODIPY **5i** with *i-azoRBC* and NADH (1:1 EtOH/TRIS buffer at pH 7.0). The 100% absorbance at 615 nm corresponds to 0.3 a.u.

Table 1. Enzymatic Reductive Cleavage of N═N of Azocompounds

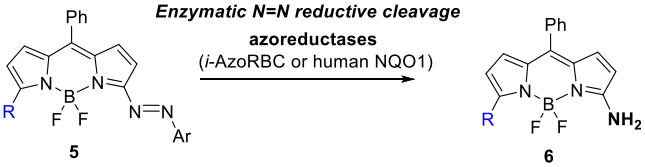

			activity[a] (%)[b]	
entry	azo	λ_{abs} (nm)	*i-azoRBC*	NQO1
1	methyl red	430	4 (100)	2 (100)
2	**5i**	615	4 (100)	0.6 (30)
3	**3**	608	3.2 (80)	1 (50)
4	**5c**	610	5 (125)	3.4 (170)
5	**5e**	614	1.2 (30)	1 (50)
6	**5f**	616	4.4 (110)	0.5 (25)
7	**5g**	630	2 (51)	1.4 (70)

[a]Activity = μmoles/min of reduced azocompound per mg of the enzyme used. [b]Activity percentage considering 100% the activity with methyl red.

The reductive cleavage of azo-BODIPY was also tested with less accessible human enzyme NADH-quinone oxido-reductase (NQO1), and the activity was compared with the immobilized *i-azoRBC* (Table 1). NQO1 is a dimeric redox enzyme (with 30,000 kDa per subunit), dependent on the FAD cofactor and present in a large number of solid tumors in all types of organisms.[23] NQO1 contains two active centers that are capable of giving up four electrons to reduce and break azo bonds and convert them into two amines. The reduction with NQO1 should be carried out in a completely aqueous media, and therefore, the concentration of azo-BODIPY **5** was required to decrease from 25 to 2.5 μM. Methyl red was also taken as a reference and considered as the 100% of the activity percentage (Table 1, NQO1 column, entry 1).

Finally, we evaluated the potential use of the azo-BODIPY **5i** as turn-on fluorescent biosensors in living cells. The initial toxicity studies were evaluated using the MTT assay,[24] incubating HeLa cells for 2 h with both compounds, azo-BODIPY **5i** and the reduction product **6i**, at different concentrations (2, 5, 10, and 20 μM in complete medium, using DMSO as a cosolvent). The survival rates after 24 h showed no significant toxicity at concentrations up to 20 μM for both derivatives (Figure S17).

Live cell imaging studies were performed using **5i** in HeLa cells gradually subjected to an oxygen free atmosphere.[25] It has

https://doi.org/10.1021/jacs.2c01197
J. Am. Chem. Soc. 2022, 144, 8185−8193

been reported that the thin cover glass placed over a cell culture plate blocks the oxygen supply to the cells beneath it, resulting in a decrease of oxygen concentration and generating anoxia or different levels of hypoxia.[10a,b,26] Under such conditions, the azo-based fluorescent quenchers release the fluorophore upon cleavage of the N═N double bond by the inside cell azoreductases. In our case, HeLa cells were dosed with azo-BODIPY **5i** (10 μM) and incubated for 2 h.[27] Then, the cells grown on coverslips, were placed on slides, and analyzed under a fluorescence microscope at different times (0, 10, 20, and 40 min). The fluorescence imaging studies revealed a red intracellular fluorescence increase under this oxygen-deprived condition (Figure 6A, +AZO). HeLa cells under the same

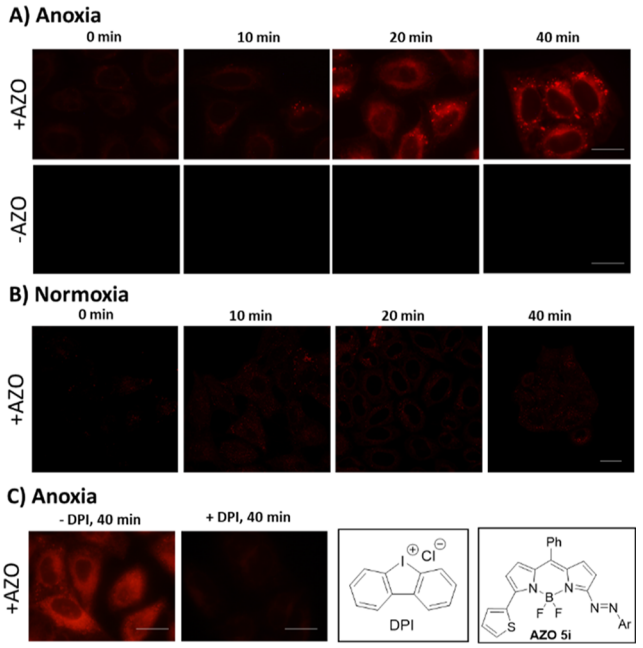

Figure 6. (A) Fluorescence images of HeLa cells incubated for 2 h with **5i** (+AZO) 10 μM and without **5i** (−AZO) and subjected to different oxygen deprivation times (10, 20, and 40 min). (B) Confocal images of HeLa cells incubated with **5i** for 2 h under normoxia at different times. (C) Fluorescence images of HeLa cells incubated with **5i** without DPI (−DPI) and with 10 μM DPI (+DPI) for 2 h and subjected to 40 min of oxygen deprivation time. The fluorescent images were obtained under green light excitation. The confocal images were obtained using excitation at 561 nm. Scale bar: 20 μM.

oxygen-deprived condition but without **5i** showed no fluorescent signal (Figure 6A, −AZO). We tested the selectivity of **5i** under normoxic conditions (without the cover glass on top) and no fluorescence increase occurred (Figure 6B). (For the quantification of fluorescence intensity, see Figure S18).

Moreover, the inhibition of the azoreductase activity, using DPI (10 μM, diphenyleneiodonium chloride),[28,29] under anoxic conditions (40 min) revealed no fluorescence increase (Figure 6C). All these results indicate that azo **5i** is reduced by reductases and help selectively differentiate between normoxic and anoxic conditions inside the HeLa cells.

In conclusion, a family of 3-arylazo-BODIPY dyes as novel fluorescent quenchers has been prepared. Our design allowed for an easy conjugation of the BODIPY fluorophore directly to the azo moiety under very mild conditions, complementary to the usual azo-coupling reaction that requires the preparation of diazonium salts. Our approach also allowed for the final tuning of the electronic properties of the BODIPY by the Suzuki cross-coupling reaction of different aryl and heteroaryl groups at C-5. The azo moiety is able to extinguish the emission of the BODIPY by a nonradiative process operating under a non-FRET mechanism. Our calculations predict that the coupling of azobenzene to the BODIPY triggers a restructuration of the topography of the S_1 potential energy surface by substituting the deep minimum responsible for the fluorescence in the parent BODIPY compound for two shallow minima in the azo-BODIPY. From these minima, of $\pi\pi^*$ or $n\pi^*$ character, the access of two internal conversion funnels is thermodynamically feasible, allowing for the return of the population to the ground state. The absence of the cis-isomer during the experimental photoisomerization studies at different wavelengths discards the usual ultrafast trans/cis deactivation pathway and suggested that only the unreactive $n\pi^*$ pathway is operative. The reduction of this azo-BODIPY allows us to access to 3-amino-BODIPY derivatives that possess a strong absorption in the green-red region, with large molar absorption coefficients and relatively large stokes shifts. The amino-BODIPY species are governed by an excited state potential energy profile, where nonnegligible energy barriers preclude the access of the internal conversion funnels to the ground state, which translate into fluorescence emission. Moreover, an immobilized bacterial azoreductase (*i-azoRBC*) protocol has been probed as a reliable model to study the azo-reducing capacity of less accessible human reductase NQO1, present in solid tumors. These results are very promising for future biological applications, as it would allow the most suitable azo compound to be selected following a simple enzymatic activity assay. The azo bond was reductively cleaved under enzymatic conditions and also in HeLa cells lacking oxygen, proving its potential application as turn-on fluorescent hypoxia probes.

■ ASSOCIATED CONTENT

Supporting Information

The Supporting Information is available free of charge at https://pubs.acs.org/doi/10.1021/jacs.2c01197.

Experimental procedures, UV−vis and emission spectra, fluorescence quantum yields, additional computational and enzymatic details, fluorescence microscopy images, fluorescence intensity quantification, ^{1}H and ^{13}C NMR spectra of all compounds (PDF)

■ AUTHOR INFORMATION

Corresponding Authors

José Manuel Guisán − *Departamento de Biocatálisis, Instituto de Catálisis y Petroquímica (CSIC), 28049 Madrid, Spain;* orcid.org/0000-0003-1627-6522; Email: jmguisan@icp.csic.es

Inés Corral − *Departamento de Química, Facultad de Ciencias and Institute for Advanced Research in Chemical Sciences (IAdChem), Universidad Autónoma de Madrid, 28049 Madrid, Spain;* orcid.org/0000-0002-9455-4906; Email: ines.corral@uam.es

Francisco Sanz-Rodriguez − *Departamento de Biología, Facultad de Ciencias, Universidad Autónoma de Madrid, 28049 Madrid, Spain;* orcid.org/0000-0002-9977-6102; Email: francisco.sanz@uam.es

Maria Ribagorda − *Departamento de Química Orgánica, Facultad de Ciencias and Institute for Advanced Research in Chemical Sciences (IAdChem), Universidad Autónoma de*

https://doi.org/10.1021/jacs.2c01197
J. Am. Chem. Soc. 2022, 144, 8185−8193

Madrid, 28049 Madrid, Spain; orcid.org/0000-0001-7185-4095; Email: maria.ribagorda@uam.es

Authors

Santiago Guisán-Ceinos − *Departamento de Química Orgánica, Facultad de Ciencias, Universidad Autónoma de Madrid, 28049 Madrid, Spain*

Alexandra R. Rivero − *Departamento de Química Orgánica, Facultad de Ciencias, Universidad Autónoma de Madrid, 28049 Madrid, Spain;* orcid.org/0000-0002-0762-6044

Fernando Romeo-Gella − *Departamento de Química, Facultad de Ciencias, Universidad Autónoma de Madrid, 28049 Madrid, Spain;* orcid.org/0000-0002-7991-781X

Silvia Simón-Fuente − *Departamento de Química Orgánica, Facultad de Ciencias, Universidad Autónoma de Madrid, 28049 Madrid, Spain;* orcid.org/0000-0002-3202-9196

Silvia Gómez-Pastor − *Departamento de Biología, Facultad de Ciencias, Universidad Autónoma de Madrid, 28049 Madrid, Spain;* orcid.org/0000-0003-1571-8368

Natalia Calvo − *Departamento de Biología, Facultad de Ciencias, Universidad Autónoma de Madrid, 28049 Madrid, Spain;* orcid.org/0000-0002-5091-7832

Alejandro H. Orrego − *Departamento de Biocatálisis, Instituto de Catálisis y Petroquímica (CSIC), 28049 Madrid, Spain;* orcid.org/0000-0003-4412-1579

Complete contact information is available at: https://pubs.acs.org/10.1021/jacs.2c01197

Author Contributions

S.G.-C. and A.R.R. contributed equally. All authors have given approval to the final version of the manuscript.

Notes

The authors declare no competing financial interest.

■ ACKNOWLEDGMENTS

This article is dedicated to Professor M. Carmen Carreño on the occasion of her retirement. We thank MINECO (grant CTQ2017-85454-C2-2-P), MICINN (grant PID2020-113059GB-C22), MCIU (grant PGC2018-094644-B-C21), the Ramón y Cajal Program (grant RYC-2016-20489), the Fundación La Caixa (grant no. LCF/BQ/DR19/11740024), and the Comunidad Autónoma de Madrid (B2017/BMD-3867 RENIMCM) and co-financed by the European Structural and investment fund for financial support. I.C. and F.R.-G. also acknowledge the Red Española de Supercomputación, the MareNostrum Supercomputer Center, and the Centro de Computación Científica of the UAM (CCC-UAM) for the generous allocation of computer time and for their technical support. We thank the "Servicio de Microscopía óptica y confocal CBMSO" facility for their assistance. We also thank Prof. M. C. Carreño for her advice and helpful discussions during the work.

■ REFERENCES

(1) Chevalier, A.; Renard, P.-Y.; Romieu, A. Azo-Based Fluorogenic Probes for Biosensing and Bioimaging: Recent Advances and Upcoming Challenges. *Chem.—Asian J.* **2017**, *12*, 2008−2028.

(2) Santos, F. d. S.; Descalzo, R. R.; Gonçalves, P. F. B.; Benvenutti, E. V.; Rodembusch, F. S. Evidence for Excited State Intramolecular Charge Transfer in Benzazole-Based Pseudo-Stilbenes. *Phys. Chem. Chem. Phys.* **2012**, *14*, 10994−11001.

(3) (a) Poprawa-Smoluch, M.; Baggerman, J.; Zhang, H.; Maas, H. P. A.; De Cola, L.; Brouwer, A. M. Photoisomerization of Disperse Red 1 Studied with Transient Absorption Spectroscopy and Quantum Chemical Calculations. *J. Phys. Chem. A* **2006**, *110*, 11926−11937. (b) Bandara, H. M. D.; Burdette, S. C. Photoisomerization in Different Classes of Azobenzene. *Chem. Soc. Rev.* **2012**, *41*, 1809−1825.

(4) Misal, S. A.; Gawai, K. R. Azoreductase: A Key Player of Xenobiotic Metabolism. *Bioresour. Bioprocess.* **2018**, *5*, 17.

(5) (a) Ranasinghe, R. T.; Brown, T. Fluorescence Based Strategies for Genetic Analysis. *Chem. Commun.* **2005**, 5487−5502. (b) Haugland, R. P. *The Handbook: A Guide to Fluorescent Probes and Labeling Technologies*, 11th ed.; Invitrogen: Oregon, 2006. (c) Drake, C. R.; Miller, D. C.; Jones, E. F. Activatable Optical Probes for the Detection of Enzymes. *Curr. Org. Synth.* **2011**, *8*, 498−520.

(6) Kiyose, K.; Hanaoka, K.; Oushiki, D.; Nakamura, T.; Kajimura, M.; Suematsu, M.; Nishimatsu, H.; Yamane, T.; Terai, T.; Hirata, Y.; Nagano, T. Hypoxia-Sensitive Fluorescent Probes for in Vivo Real-Time Fluorescence Imaging of Acute Ischemia. *J. Am. Chem. Soc.* **2010**, *132*, 15846−15848.

(7) Eltzschig, H. K.; Carmeliet, P. Hypoxia and Inflammation. *N. Engl. J. Med.* **2011**, *364*, 656−665.

(8) (a) Wilson, W. R.; Hay, M. P. Targeting Hypoxia in Cancer Therapy. *Nat. Rev. Cancer* **2011**, *11*, 393−410. (b) Sharma, A.; Arambula, J. F.; Koo, S.; Kumar, R.; Singh, H.; Sessler, J. L.; Kim, J. S. Hypoxia-Targeted Drug Delivery. *Chem. Soc. Rev.* **2019**, *48*, 771−813.

(9) Kumari, R.; Sunil, D.; Ningthoujam, R. S.; Kumar, N. A. Azodyes as Markers for Tumor Hypoxia Imaging and Therapy: An up-to-Date Review. *Chem.-Biol. Interact.* **2019**, *307*, 91−104.

(10) (a) Myochin, T.; Hanaoka, K.; Komatsu, T.; Terai, T.; Nagano, T. Design Strategy for a Near-Infrared Fluorescence Probe for Matrix Metalloproteinase Utilizing Highly Cell Permeable Boron Dipyrromethene. *J. Am. Chem. Soc.* **2012**, *134*, 13730−13737. (b) Shin, N.; Hanaoka, K.; Piao, W.; Miyakawa, T.; Fujisawa, T.; Takeuchi, S.; Takahashi, S.; Komatsu, T.; Ueno, T.; Terai, T.; Tahara, T.; Tanokura, M.; Nagano, T.; Urano, Y. Development of an Azoreductase-Based Reporter System with Synthetic Fluorogenic Substrates. *ACS Chem. Biol.* **2017**, *12*, 558−563. (c) Piao, W.; Tsuda, S.; Tanaka, Y.; Maeda, S.; Liu, F.; Takahashi, S.; Kushida, Y.; Komatsu, T.; Ueno, T.; Terai, T.; Nakazawa, T.; Uchiyama, M.; Morokuma, K.; Nagano, T.; Hanaoka, K. Development of Azo-Based Fluorescent Probes to Detect Different Levels of Hypoxia. *Angew. Chem., Int. Ed.* **2013**, *52*, 13028−13032. (d) Uddin, M. I.; Evans, S. M.; Craft, J. R.; Marnett, L. J.; Uddin, M. J.; Jayagopal, A. Applications of Azo-Based Probes for Imaging Retinal Hypoxia. *ACS Med. Chem. Lett.* **2015**, *6*, 445−449. (e) Cui, L.; Shi, Y.; Zhang, S.; Yan, L.; Zhang, H.; Tian, Z.; Gu, Y.; Guo, T.; Huang, J. A NIR Turn-on Fluorescent Probe Applied in Cytochrome P450 Reductase Detection and Hypoxia Imaging in Tumor Cells. *Dyes Pigm.* **2017**, *139*, 587−592. (f) Wang, C.; Zhang, S.; Huang, J.; Cui, L.; Hu, J.; Tan, S. Novel Designed Azo Substituted Semi-Cyanine Fluorescent Probe for Cytochrome P450 Reductase Detection and Hypoxia Imaging in Cancer Cells. *RSC Adv.* **2019**, *9*, 21572−21577. (g) Cai, Q.; Yu, T.; Zhu, W.; Xu, Y.; Qian, X. A Turn-on Fluorescent Probe for Tumor Hypoxia Imaging in Living Cells. *Chem. Commun.* **2015**, *51*, 14739−14741. (h) Geng, W. C.; Jia, S.; Zheng, Z.; Li, Z.; Ding, D.; Guo, D. S. A Noncovalent Fluorescence Turn-on Strategy for Hypoxia Imaging. *Angew. Chem., Int. Ed.* **2019**, *58*, 2377−2381. (i) Luo, S.; Liu, Y.; Wang, F.; Fei, Q.; Shi, B.; An, J.; Zhao, C.; Tung, C.-H. A Fluorescent Turn-on Probe for Visualizing Lysosomes in Hypoxic Tumor Cells. *Analyst* **2016**, *141*, 2879−2882.

(11) (a) Chevalier, A.; Massif, C.; Renard, P.-Y.; Romieu, A. Bioconjugatable Azo-Based Dark-Quencher Dyes: Synthesis and Application to Protease-Activatable Far-Red Fluorescent Probes. *Chem.—Eur. J.* **2013**, *19*, 1686−1699. (b) Chevalier, A.; Hardouin, J.; Renard, P.-Y.; Romieu, A. Universal Dark Quencher Based on "Clicked" Spectrally Distinct Azo Dyes. *Org. Lett.* **2013**, *15*, 6082−6085.

(12) (a) Loudet, A.; Burgess, K. BODIPY Dyes and Their Derivatives: Syntheses and Spectroscopic Properties. *Chem. Rev.* **2007**, *107*, 4891−4932. (b) Bessette, A.; Hanan, G. S. Design, Synthesis and Photophysical Studies of Dipyrromethene-Based Materials: Insights into Their Applications in Organic Photovoltaic Devices. *Chem. Soc.*

Rev. **2014**, *43*, 3342−3405. (c) Frath, D.; Massue, J.; Ulrich, G.; Ziessel, R. Luminescent Materials: Locking π-Conjugated and Heterocyclic Ligands with Boron(III). *Angew. Chem., Int. Ed.* **2014**, *53*, 2290−2310.
(13) Carreño, M. C.; Mudarra, G. F.; Merino, E.; Ribagorda, M. Synthesis of Azobenzenes from Quinone Acetals and Arylhydrazines. *J. Org. Chem.* **2004**, *69*, 3413−3416.
(14) (a) Carreño, M. C.; García, I.; Núñez, I.; Merino, E.; Ribagorda, M.; Pieraccini, S.; Spada, G. P. Photoinduced Conformational Switch of Enantiopure Azobenzenes Controlled by a Sulfoxide. *J. Am. Chem. Soc.* **2007**, *129*, 7089−7100. (b) Núñez, I.; Merino, E.; Lecea, M.; Pieraccini, S.; Spada, G. P.; Rosini, C.; Mazzeo, G.; Ribagorda, M.; Carreño, M. C. Control of the Helical Chirality of Enantiopure Sulfinyl (*Z*)-Azobenzene-Based Photoswitches. *Chem.—Eur. J.* **2013**, *19*, 3397−3406.
(15) John, A. A.; Ramil, C. P.; Tian, Y.; Cheng, G.; Lin, Q. Synthesis and Site-Specific Incorporation of Red-Shifted Azobenzene Amino Acids into Proteins. *Org. Lett.* **2015**, *17*, 6258−6261.
(16) Dilek, Ö.; Bane, S. L. Synthesis of boron dipyrromethene fluorescent probes for bioorthogonal labeling. *Tetrahedron Lett.* **2008**, *49*, 1413−1416.
(17) Following this protocol, the amount of hydrazine hydrate could be decreased from 8.9 to 2 equiv. For the preparation of **1** see: Rohand, T.; Baruah, M.; Qin, W.; Boens, N.; Dehaen, W. Functionalisation of fluorescent BODIPY dyes by nucleophilic substitution. *Chem. Commun.* **2006**, 266−268.
(18) Rohand, T.; Qin, W.; Boens, N.; Dehaen, W. Palladium-Catalyzed Coupling Reactions for the Functionalization of BODIPY Dyes with Fluorescence Spanning the Visible Spectrum. *Eur. J. Org. Chem.* **2006**, *2006*, 4658−4663.
(19) Palladium sources, ligands and solvent screened: $Pd(PPh_3)_4$, $Pd(CH_3CN)_2Cl_2$, XPhosPdG2 or $Pd(dba)_3$; ligands: P(2-furanyl)$_3$ or P(^{t}Bu)$_3$ solvents: toluene, dioxane, DME, see Supporting Information for details.
(20) Longer reaction times gave mixtures of **5a** together with the hydrazine derivative.
(21) Peng, X.; Song, F.; Lu, E.; Wang, Y.; Zhou, W.; Fan, J.; Gao, Y. Heptamethine Cyanine Dyes with a Large Stokes Shift and Strong Fluorescence: A Paradigm for Excited-State Intramolecular Charge Transfer. *J. Am. Chem. Soc.* **2005**, *127*, 4170−4171.
(22) (a) Buyuktemiz, M.; Duman, S.; Dede, Y. Luminescence of BODIPY and Dipyrrin: An MCSCF Comparison of Excited States. *J. Phys. Chem. A* **2013**, *117*, 1665−1669. (b) Prlj, A.; Vannay, L.; Corminboeuf, C. Fluorescence Quenching in BODIPY Dyes: The Role of Intramolecular Interactions and Charge Transfer. *Helv. Chim. Acta* **2017**, *100*, No. e1700093. (c) De Vetta, M.; Corral, I. Insight into the optical properties of meso-pentafluorophenyl(PFP)-BODIPY: An attractive platform for functionalization of BODIPY dyes. *Comput. Theor. Chem.* **2019**, *1150*, 110−120. (d) Yu, J. K.; Bannwarth, C.; Liang, R.; Hohenstein, E. G.; Martínez, T. J. Nonadiabatic Dynamics Simulation of the Wavelength-Dependent Photochemistry of Azobenzene Excited to the nπ* and ππ* Excited States. *J. Am. Chem. Soc.* **2020**, *142*, 20680−20690.
(23) (a) Ross, D.; Siegel, D. NAD(P)H:Quinone Oxidoreductase 1 (NQO1, DT-Diaphorase), Functions and Pharmacogenetics. *Methods Enzymol.* **2004**, *382*, 115−144. (b) Li, R.; Bianchet, M. A.; Talalay, P.; Amzel, L. M. The three-dimensional structure of NAD(P)H:quinone reductase, a flavoprotein involved in cancer chemoprotection and chemotherapy: mechanism of the two-electron reduction. *Proc. Natl. Acad. Sci. U.S.A.* **1995**, *92*, 8846−8850.
(24) Rubinstein, L. V.; Shoemaker, R. H.; Paull, K. D.; Simon, R. M.; Tosini, S.; Skehan, P.; Scudiero, D. A.; Monks, A.; Boyd, M. R. Comparison of In Vitro Anticancer-Drug-Screening Data Generated With a Tetrazolium Assay Versus a Protein Assay Against a Diverse Panel of Human Tumor Cell Lines. *J. Natl. Cancer Inst.* **1990**, *82*, 1113−1117.
(25) HeLa cells are derived from an epidermoid carcinoma of the cervix. American Type Culture Collection (ATCC CCL-2).
(26) Takahashi, E.; Sato, M. Imaging of oxygen gradients in monolayer cultured cells using green fluorescent protein. *Am. J. Physiol.: Cell Physiol.* **2010**, *299*, C1318−C1323.
(27) The UV−vis and emission spectra of **5i** in a PBS/DMSO showed a maximum λ_{abs} at 500 nm and a λ_{em} at 585 nm (see Figure S3 for details).
(28) O'Donnell, V. B.; Smith, G.; Jones, O. Involvement of Phenyl Radicals in Iodonium Inhibition of Flavoenzymes. *Mol. Pharm.* **1994**, *46*, 778−785.
(29) Chakraborty, S.; Massey, V. Reaction of Reduced Flavins and Flavoproteins with Diphenyliodonium Chloride. *J. Biol. Chem.* **2002**, *277*, 41507−41516.

https://doi.org/10.1021/jacs.2c01197
J. Am. Chem. Soc. 2022, 144, 8185−8193